SUPPORTING INFORMATION

Manufacturing Silica Aerogel and Cryogel through Ambient Pressure and Freeze Drying

Massimigliano Di Luigi[a], Zipeng Guo[b], Lu An[a], Jason N. Armstrong[a], Chi Zhou[b,], Shenqiang Ren[a,c,d,*]*

[a] Department of Mechanical and Aerospace Engineering, University at Buffalo, The State University of New York, Buffalo, New York 14260, USA

[b] Department of Industrial and Systems Engineering, University at Buffalo, The State University of New York, Buffalo, New York 14260, USA

[c] Department of Chemistry, University at Buffalo, The State University of New York, Buffalo, NY 14260, USA

[d] Research and Education in Energy, Environment & Water (RENEW), University at Buffalo, The State University of New York, Buffalo, NY 14260, USA

* Email: chizhou@buffalo.edu; shenren@buffalo.edu

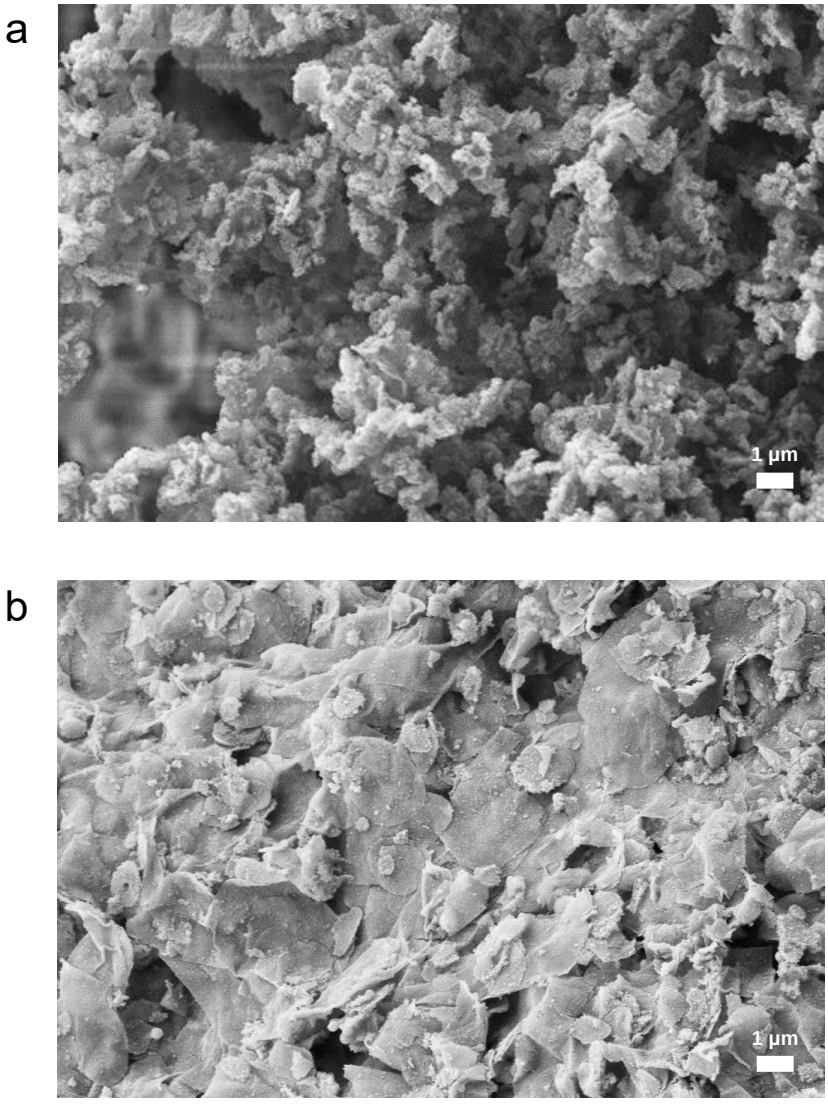

Figure S1. a) and b) SEM images (low magnification) showing typical microstructure of silica aerogels (from APD) and silica cryogels (from FD) respectively following the sintering process.

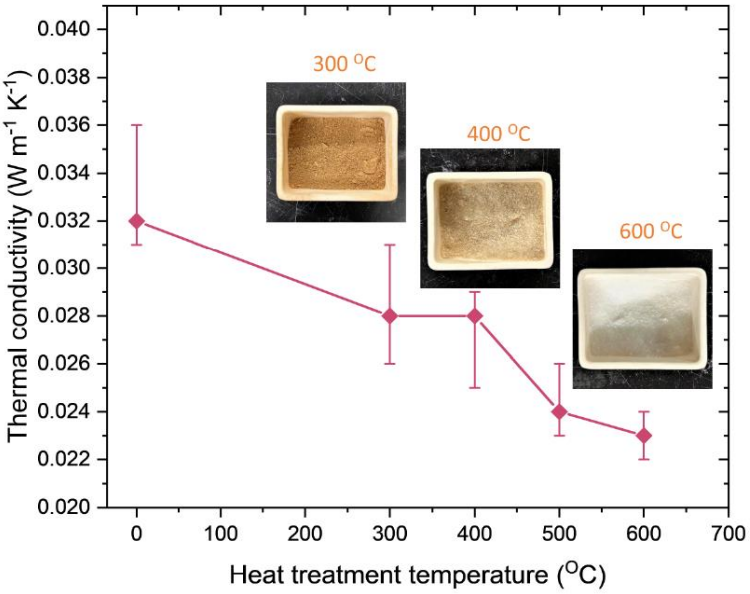

Figure S2. Thermal conductivity of freeze-dried (FD) specimens at different sintering (heat treatment) temperature.

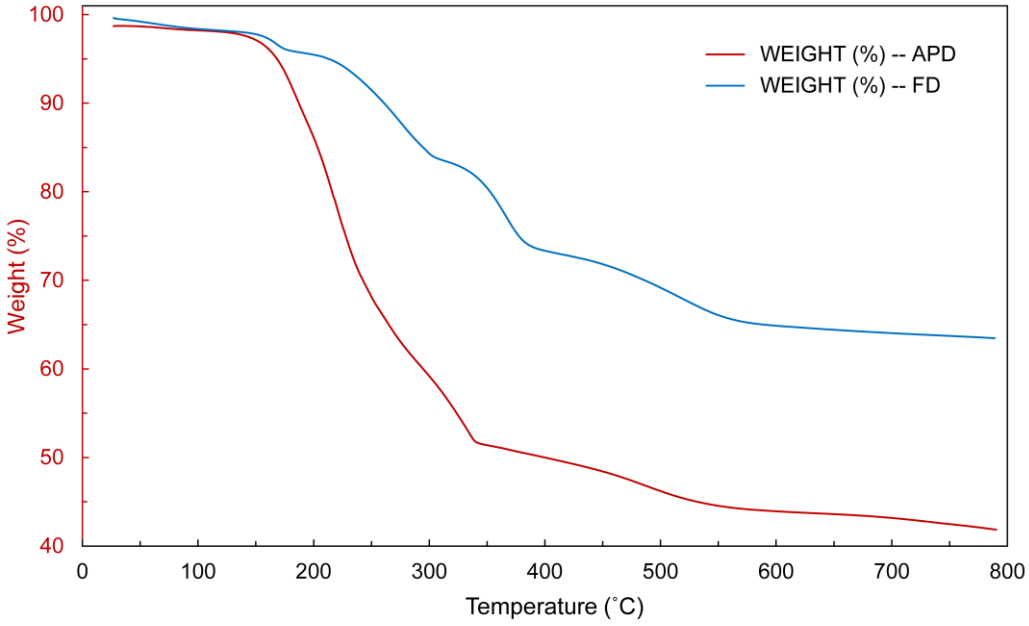

Figure S3. Weight loss % vs temperature curves (TGA test) for silica aerogel and silica cryogel specimens produced from ambient-pressure-drying (APD) and freeze-drying (FD) procedures respectively.

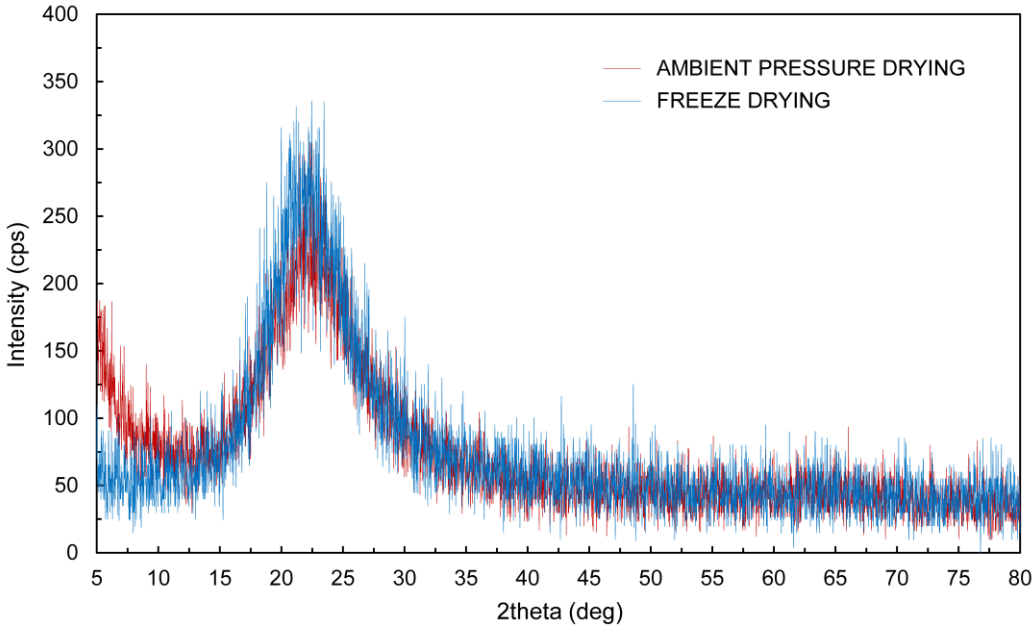

Figure S4. X-ray diffraction (XRD) spectra for silica aerogel and silica cryogel specimens produced from ambient-pressure-drying (APD) and freeze-drying (FD) procedures respectively. All samples have been sintered to 600 °C.

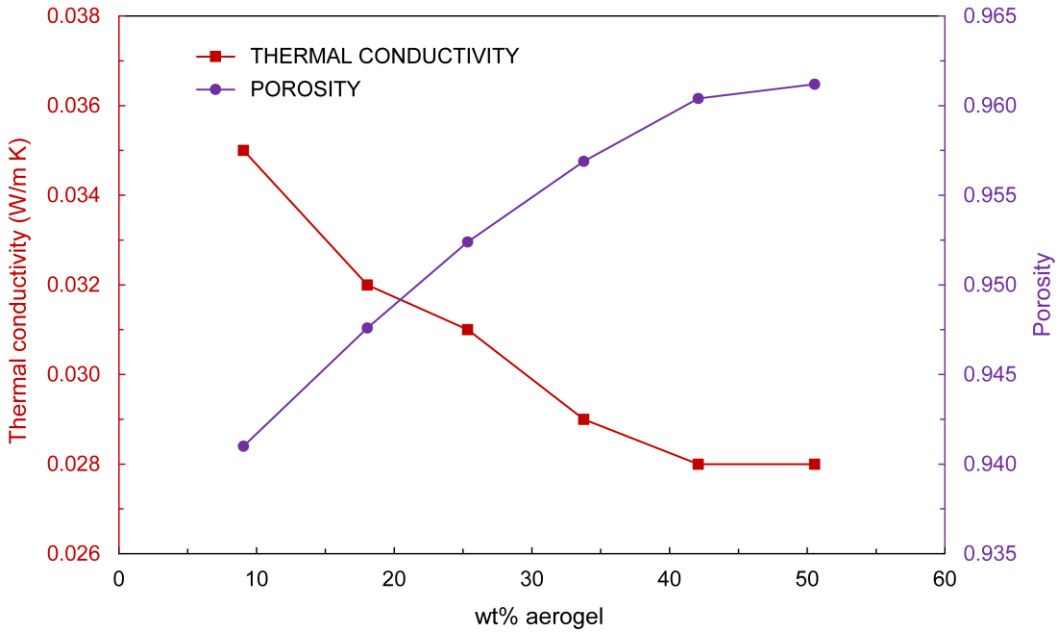

Figure S5. Thermal conductivity and porosity vs weight% of aerogel for ceramic fiber/silica cryogel composite materials obtained from the freeze-drying (FD) procedure.

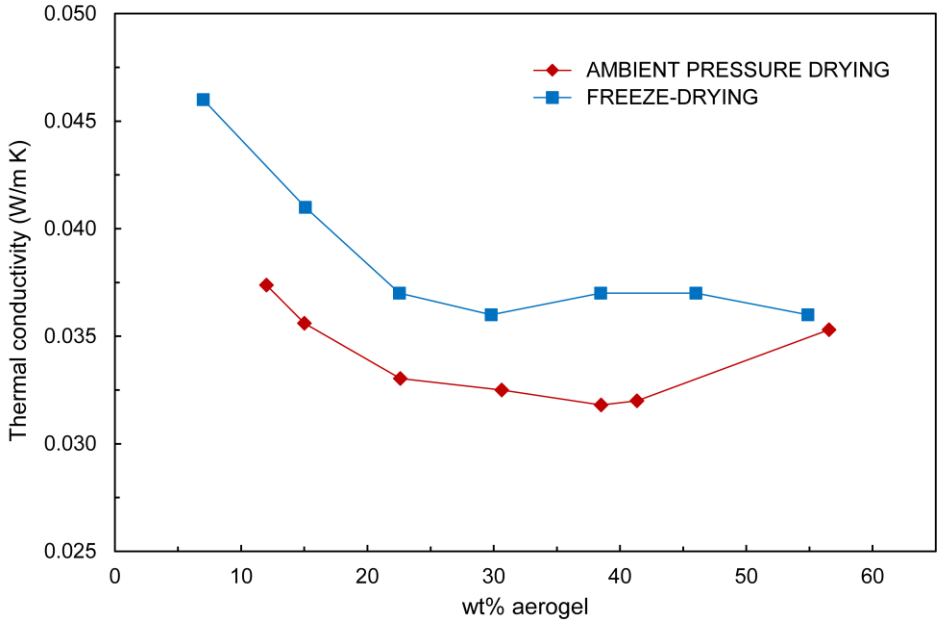

Figure S6. Thermal conductivity vs weight% of aerogel for ceramic fiber/silica cryogel and ceramic fiber/silica aerogel composite materials obtained from the freeze-drying (FD) and ambient-pressure-drying (APD) procedures.

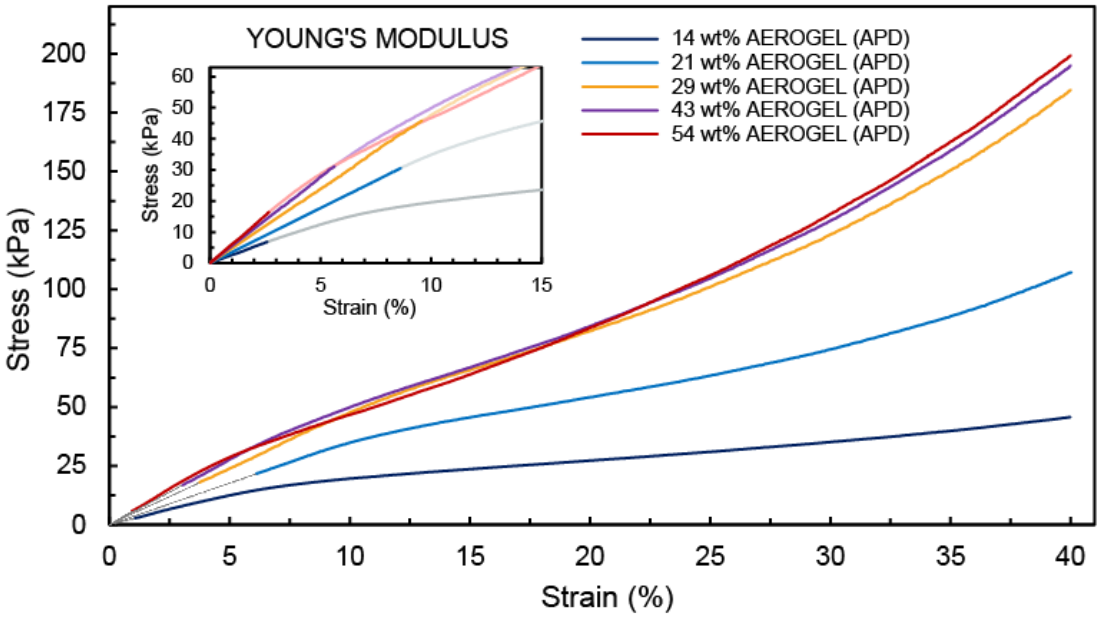

Figure S7. Strain vs stress from uniaxial compression tests on composite materials (ceramic-fiber/silica aerogel) obtained from the ambient-pressure-drying (APD) procedure with different wt% of aerogel.

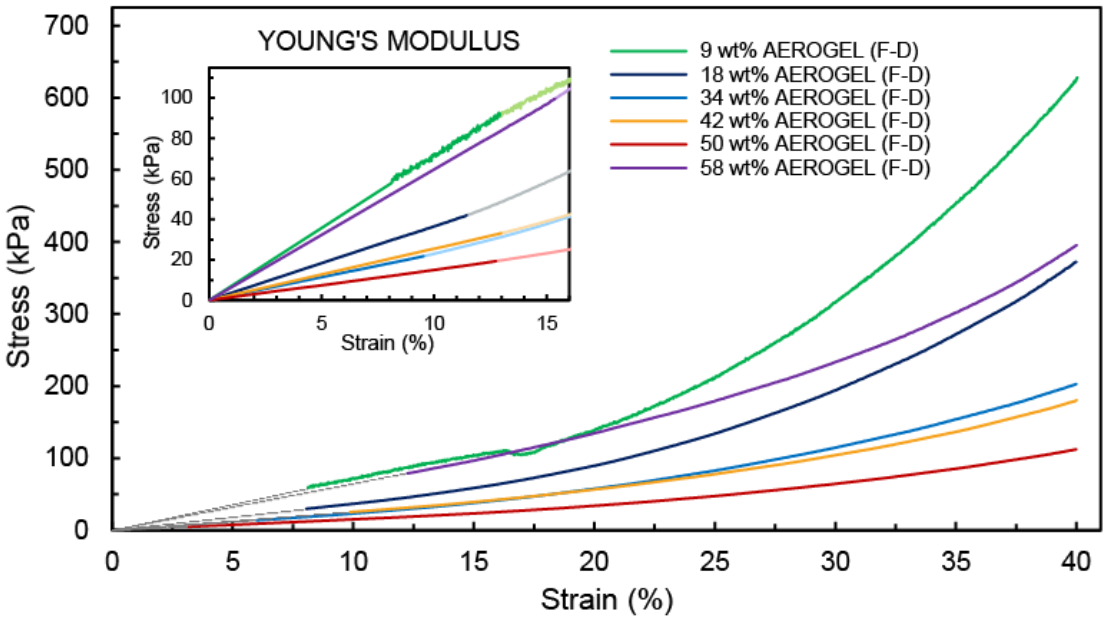

Figure S8. Strain vs stress from uniaxial compression tests on composite materials (ceramic-fiber/silica cryogel) obtained from the freeze-drying (APD) procedure with different wt% of aerogel.

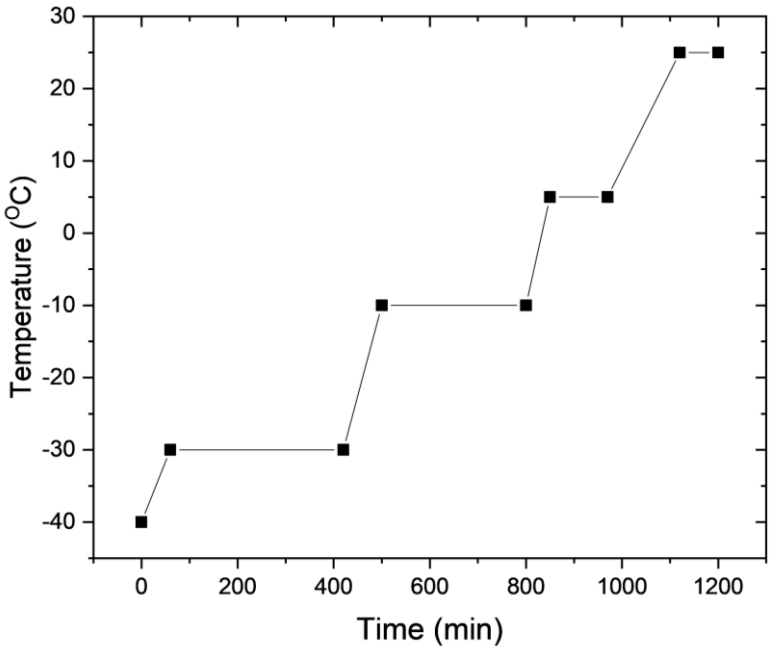

Figure S9. Temperature profile during the freeze-drying (FD) procedure.

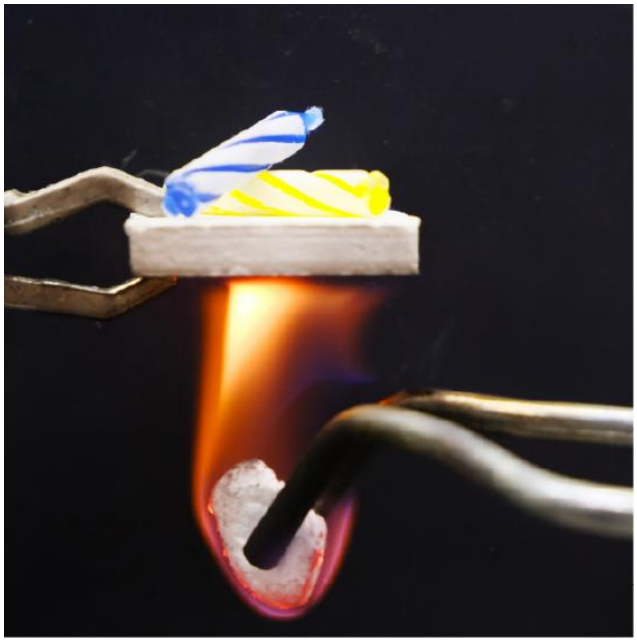

Figure S10. Flame-retardant capabilities of composite materials (ceramic-fibre/silica cryogel) from freeze-drying (FD) procedure.

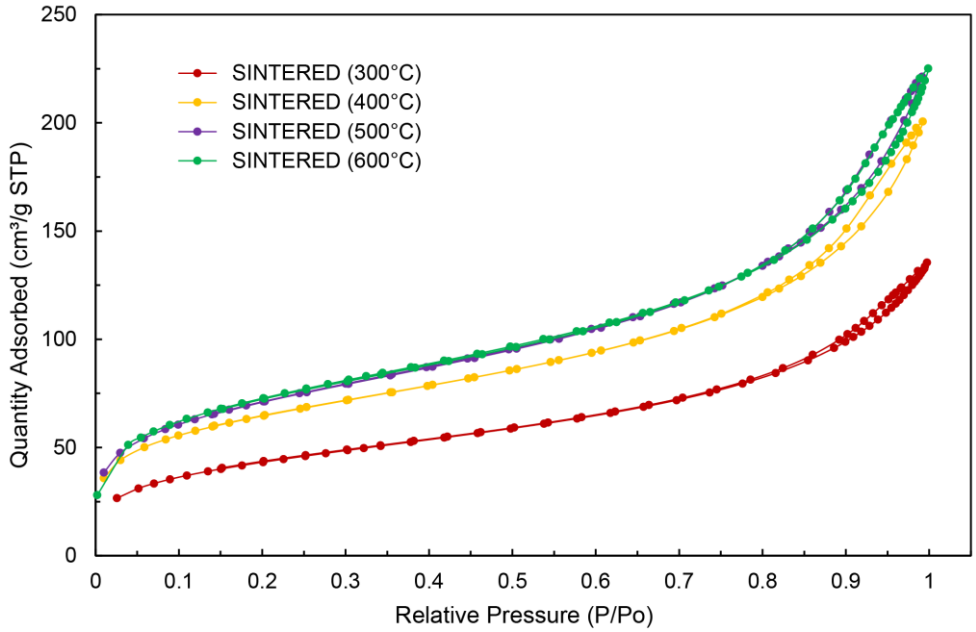

Figure S11. Isotherm curves from BET/BJH tests on aerogel materials from ambient pressure drying at different sintering temperatures. *(Aerogel precursor: 1:1 SDS/CTAB | 6.875 mol/L urea | 25wt% Ion-exchanged waterglass)*

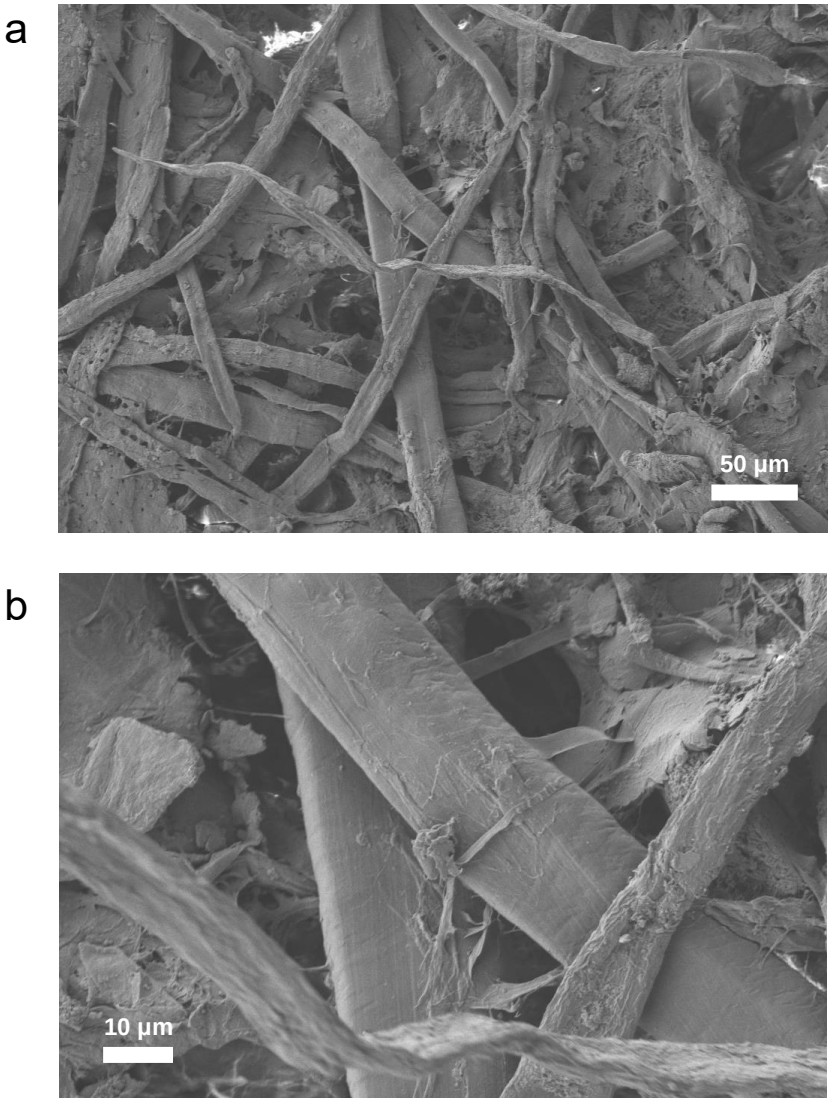

Figure S12. SEM images (a – low magnification; b – high magnification) showing typical microstructure of a pure cellulose fiber specimen (no aerogel precursor has been used for this sample).

Table S1. Properties of aerogel specimens obtained from ambient pressure drying (APD) procedure following sintering to different temperatures. *(Aerogel precursor: 1:1 SDS/CTAB | 6.875 mol/L urea | 25wt% Ion-exchanged waterglass)*

SINTERING TEMPERATURE *(°C)*	**k** *($W \cdot m^{-1} \cdot K^{-1}$)*	**BET SSA** *(m^2/g)*	**BJH DESORPTION AVG. PORE WIDTH** *(nm)*
300	0.02578	191.61	7.093
400	0.02551	226.76	6.936
500	0.02503	279.97	6.455
600	0.02496	290.02	6.713

Table S2. Mechanical properties following uniaxial compression tests on composite materials obtained from both ambient pressure drying (APD) and freeze-drying (FD) procedures.

AMBIENT PRESSURE DRYING			**FREEZE-DRYING**		
wt% AEROGEL *(%)*	MAX. COMPRESSIVE STRESS AT 40% STRAIN *(kPa)*	YOUNG'S MODULUS *(kPa)*	wt% AEROGEL *(%)*	MAX. COMPRESSIVE STRESS AT 40% STRAIN *(kPa)*	YOUNG'S MODULUS *(kPa)*
13.8	45.7	266.6	9.1	625.2	714.6
21.2	107.2	353.3	18.1	372.2	367.9
29.1	184.6	478.6	33.8	202.5	165.0
43.0	194.9	553.4	42.1	180.3	180.9
54.3	199.2	611.8	50.5	112.4	107.4